

(1)First page

classification of paper : Original Paper

paper title : Analyzing the Components of Dark Circle by Nonlinear Estimation of Chromophore Concentrations and Shading

author names : Rina Akaho, Misa Hirose and Norimichi Tsumura

affiliation :

Graduate School of Advanced Integration Science, Chiba University

address : 1-33, Yayoi-cho, Inage-ku, Chiba-shi, Chiba, 263-8522 Japan

E-mail address : akaho@chiba-u.jp

(2) Abstract

This paper aims to apply nonlinear estimation of chromophore concentrations: melanin, oxy-hemoglobin, deoxy-hemoglobin and shading to the real hyperspectral image of skin. Skin reflectance is captured in the wavelengths between 400nm and 700nm by hyperspectral scanner.

Five-band wavelengths data are selected from skin reflectance.

By using the cubic function which obtained by Monte Carlo simulation of light transport in multi-layered tissue, chromophore concentrations and shading are determined by minimize residual sum of squares of reflectance. The dark circles are analyzed by the proposed method, and dominant component of the dark circles is found by the subjective evaluation for the modulated images.

(3) Keywords

melanin volume, blood volume, Monte Carlo simulation, spectral reflectance

(4) Main text

1. Introduction

Multispectral imaging has generated growing interest in various fields, such as biomedical imaging, recording for digital archives, and sensing and controlling systems in the last few decades¹⁻⁹. The main aim of image sensing is to provide non-contact and non-invasive sensing techniques.

Skin is a multi-layered tissue composed of the epidermis, dermis and subcutaneous tissues and contains chromophores such as melanin, oxy-hemoglobin and deoxy-hemoglobin. Since diffuse reflectance of human skin is changed depending on the concentration of these chromophores, the analysis of diffuse reflectance can provide information about tissue activities related to these chromophores. This information is useful to be applied for early detection of skin disease and monitoring health.

Tsumura *et al.* discussed a method of extracting melanin and hemoglobin information by applying Independent Component Analysis (ICA) to skin color images^{1,5}. Kikuchi *et al.* proposed imaging of a hemoglobin oxygen saturation ratio of the face with a spectral camera based on the multi regression analysis¹⁰. There are many discussions about estimating chromophore concentrations linearly from skin color images and spectral images. On the other hand, Kobayashi *et al.* analyzed the nonlinear relation between absorbance and chromophores of skin based on Monte Carlo simulation and the modified Lambert-Beer's law¹¹. Kobayashi *et al.* reported a method of estimating the optical path length of each layer from absorbance and the quantity of chromophores.

By using the estimated optical path length, the concentration of chromophores can be analysed based on the modified Lambert-Beer's law. However, this method cannot estimate the optical path length if the concentration of chromophores is not provided.

Even if the concentration is supplied, the estimation accuracy is not sufficient because the concentration is derived linearly by multiple regression analysis. Hirose *et al.* calculated the relationship between chromophore concentration and absorbance by creating the combination of a chromophore concentration on the simulation¹². Estimation accuracy of the method by Hirose *et al.* was evaluated by numerical skin phantom, they concluded that their method performed high accurate estimation. However it was not applied and evaluated by real skin images.

2. Nonlinear Estimation of Chromophore Concentrations and Shading from Five Band Images ⁹⁾

2.1 Analysis of the Relation between Absorbance and Chromophore Concentration

First, we analyze the relation between absorbance and chromophore concentration by Monte Carlo simulation and define the absorbance as the cubic functions of chromophore concentration as it was previously performed by minimizing ¹¹⁾.

Diffuse reflectance data for skin is obtained by Monte Carlo simulation of light transport in multi-layered tissue (MCML) ⁹⁾. MCML follows the propagation of photons in tissue.

As shown in Fig. 1, the two-layered skin model is used and is composed of the epidermis and dermis.

Five optical parameters are set at each layer: thickness t , reflectance index n , anisotropy factor g , scattering coefficient μ_s , and absorption coefficient μ_a . The thickness t of epidermis and dermis are 0.006 and 0.40 cm respectively in this basic model ¹³⁾. The reflectance index n , scattering coefficient μ_s , and anisotropy factor g of two layers are the same value, $n = 1.4$, μ_s and g is based on previously used data ⁴⁾. The absorption coefficient μ_a is calculated by the absorption coefficients of chromophores such as melanin, oxy-hemoglobin and deoxy-hemoglobin as follows.

$$\begin{aligned}\mu_{a,epi}(\lambda) &= Mel \times 0.01 \times \mu_{a,mel}(\lambda), \\ \mu_{a,der}(\lambda) &= \{Ohb \times \mu_{a,ohb}(\lambda) + Hb \times \mu_{a,hb}(\lambda)\} \times 0.01 \\ &= \{Thb \times StO \times \mu_{a,ohb}(\lambda) + Thb \times (1 - StO) \times \mu_{a,hb}(\lambda)\} \times 0.01,\end{aligned}\tag{1}$$

where λ is the wavelength and the subscripts of the absorption coefficient epi , der , mel , ohb , and hb indicate epidermis, dermis, melanin, oxy-hemoglobin, and deoxy-hemoglobin, respectively. Mel , Ohb , Hb , Thb and StO indicate concentration of melanin, oxy-hemoglobin, deoxy-hemoglobin and oxygen saturation, respectively.

Chromophore concentrations are input to MCML to acquire diffuse reflectance of skin. Set melanin concentration $Mel = 0.01, 0.02, 0.03, 0.04, 0.05, 0.06, 0.07, 0.08, 0.09$ and 0.1 ; $Thb = 0.002, 0.004, 0.006, 0.008$ and 0.01 ; and $StO = 0, 0.2, 0.4, 0.6, 0.8$ and 1 . 300 reflectance data are obtained from their combinations.

The diffuse reflectance obtained by MCML is converted to absorbance with logarithmic transformation, and the absorbance for each wavelength is defined by a cubic function of chromophore concentration. The chromophore concentration is determined to minimize the residual sum of squares of the reflectance as is described in next section.

2.2 Estimation of Chromophore Concentrations and Shading from Five Band Images

Four components, melanin, oxy-hemoglobin, deoxy-hemoglobin and shading, are extracted from five band images of the skin by using cubic functions. For this purpose, these four components are determined to minimize the residual sum of squares RSS_{est} as follows.

$$RSS_{est} = \sum [R(\lambda) - (\exp(-(Z(\lambda) + k)))]^2, \quad (2)$$

where $R(\lambda)$ is spectral reflectance of human skin and k indicate bias value which is shading component. $Z(\lambda)$ is absorbance defined by the cubic function of melanin concentration and absorption coefficient of dermis.

$$Z = aX^3 + bX^2Y + cXY^2 + dY^3 + eX^2 + fXY + gY^2 + hX + iY + j, \quad (3)$$

where $a \sim j$ are absorption coefficient. X is absorption coefficient of dermis and Y is percentage of melanin. Fig.2 shows $Z(\lambda)$ in case the wavelength is 700nm. Estimation accuracy of the method by Hirose *et al.* was evaluated by numerical skin phantom, they concluded that their method performed high accurate estimation ¹²⁾. In the next section, therefore, we apply this method to the real skin spectral image.

3. Estimation of Chromophore Concentrations and Shading from Real Images

3.1 Experimental Environment and Selection of Wavelengths set

Fig.4 shows experimental set-up to capture hyperspectral images of skin. Hyperspectral images were captured using a hyperspectral scanner(JFE ImSpector) in every 10nm between 400nm and 700nm and using artificial solar(Seric Ltd.) as a light source in a dark room. Surface reflectance is removed to improve the accuracy for estimation of chromophore concentrations and shading. In this experiment, Spectralon was used as a white checker. This white checker is close to the perfectly diffusing surface and size is 300mm×40mm×10mm. First, we captured hyperspectral image of white checker. Reflected spectral power of skin is divided by reflected spectral power of white checker to obtain spectral reflectance of skin. Fig.5 shows the RGB images which is converted from spectral reflectance of skin. We used 10-degree color-matching function and standard illumination light D65 as a light source for conversion to RGB image. We empirically selected 5 wavelengths from the obtained 31 wavelengths data, and estimation chromophore concentrations by using the method describe in section 2.2. Appropriate wavelengths set are determined to minimize the residual sum of squares RSS_{wav} as follows.

$$RSS_{est} = \sum_{c=1}^N \sum_{\lambda} [R_{est}(\lambda) - R_{real}(\lambda)]^2, \quad (4)$$

where $R_{est}(\lambda)$ is spectral reflectance calculated from estimated five components and $R_{real}(\lambda)$ is spectral reflectance captured using a hyperspectral scanner. N is the number of pixels in the image.

3.2 Results and Discussion

Appropriate wavelengths set were 470, 510, 570, 630, 700nm from our results of evaluating using Eq.(3). Fig. 6 shows results of estimation at images including pigmented spot on the skin. Melanin concentration map is shown in Fig. 6(a). It is estimated that melanin concentration is high density at pigmented spot area on the skin. Fig. 8 shows the result of estimation on dark circles under the eyes. It is also estimated that melanin concentration is high density at the freckle area and the area of dark circles. Shading map is shown in Fig. 8(b). From this result, it is observed that the shading components are estimated appropriately on the aspect of the shape trend in the area. Fig. 8(c) shows oxygen saturation map. From this result, it is observed that oxygen saturation is low at dark circles area under the eyes. Fig. 7 and Fig. 9 show the result of estimation by using conventional multiple regression analysis. Results of both area seem to be estimated appropriately, however, melanin concentration and blood volume are very low and oxygen saturation are very noisy^{13), 14)}.

4. Modulating chromophore concentration

Estimated chromophore concentrations which are obtained from previous section are modulated. The modulated concentrations are used to calculate the spectral reflectance as in the Section 2.2. RGB images are calculated from the spectral reflectance. Furthermore, RGB images of dark circles are evaluated to determine dominant components relating appearance of dark circles.

4.1 Modulation of estimated concentration value

First, threshold is set for each component; melanin, blood volume, oxygen saturation and shading. In melanin and shading if the estimated concentration at one pixel is higher than threshold value, the component is modulated by image processing. In blood volume and oxygen saturation, if estimated concentration at one pixel is lower than threshold, the component is modulated by image processing. The concentrations are modulated as follows.

$$Mel_{control} = Mel + P_{Mel} \times (Mel_{max} - Mel_{min}) \quad (5)$$

$$StO_{control} = StO + P_{StO} \times (StO_{max} - StO_{min}) \quad (6)$$

$$Thb_{control} = Thb + P_{Thb} \times (Thb_{max} - Thb_{min}) \quad (7)$$

$$Sha_{control} = Sha + P_{Sha} \times (Sha_{max} - Sha_{min}) \quad (8)$$

where Mel , StO , Thb , Sha are estimated concentrations at the pixel under the modulation. P_{Mel} , P_{StO} , P_{Thb} , P_{Sha} are degree of modulation. Mel_{max} , StO_{max} , Thb_{max} , Sha_{max} are maximum value in estimated area and Mel_{min} , StO_{min} , Thb_{min} , Sha_{min} are minimum value. We use three types about degree of modulation; unchanging, decreasing and increasing as Fig.10. Since there are four components in the images and three types of modulation in the image processing, we obtained 81 images from combinations. Fig.11-13 shows example of modulated images.

4.2 Generation of RGB image for evaluation

Absorbance of modulated chromophore concentrations is defined by concentrations using Eq.3. Absorbance is converted into reflectance using Eq.9. RGB image is obtained from reflectance and performed gamma correction for sRGB display.

$$R(\lambda) = \exp(-Z(\lambda) + k), \quad (9)$$

5. Removal of dark circles

5.1 Subjective evaluation experiment for finding dominant component of dark circles

Fig. 14(a) shows experimental setup of evaluation experiment. Example of evaluated images are shown in Fig. 14(b). Left image is before modulation and right side is the image after modulation. The observers are asked to evaluate the image after modulation compared with the image before modulation. The evaluation is performed by classification with five grades as Table 1. In the evaluated images, only the area in green rectangle is modulated in this paper.

5.2 Result of subjective evaluation experiment

Result of experiment for subjective evaluation shown in Fig. 15. Horizontal axis is number of evaluated image, it is sorted by modulation degree of melanin. Vertical axis is value in average evaluation. When the one component is fixed, there are 27 combinations. Fig. 15 shows that melanin component is highly related to appearance of dark circles in this experiment. Although the evaluation value is changed by combination of other three components, it can be said the difference in each groups; unchanged, decreased, increased, can be ignored as seen in Fig. 15. Moreover, significant difference test by using variance analysis showed that only melanin affected the appearance.

6. Conclusion

We estimated chromophore concentrations from hyperspectral image of skin by using nonlinear estimation method. As a result of melanin concentration map, melanin was high concentration at pigmented spot, freckle and dark circles. At dark circle area, oxygen saturation was low concentration. From these results, we can conclude that the method by Hirose *et al.* can be applied to real skin images since physiologically valid results were obtained by our study. Furthermore, we modulated estimated concentration and found melanin component is highly related to appearance of dark circles. In future works, we will apply this method for many kinds of dark circles.

References

- 1) N. Tsumura, H. Haneishi, and Y. Miyake, *J. Opt. Soc. Am. A*, vol. 16, pp. 2169-2176 (1999).
- 2) Y. Miyake, Y. Yokoyama, N. Tsumura, H. Haneishi, K. Miyata and J. Hayashi, *Proc. SPIE*, vol. 3648, pp. 218-225(1999).
- 3) H. Haneishi, T. Hasegawa, A. Hosoi, Y. Yokoyama, N. Tsumura, and Y. Miyake, *Appl. Opt.*, vol. 39, pp. 6621-6632(2000).
- 4) N. Tsumura, M. Kawabuchi, H. Haneishi and Y. Miyake, *J. Imaging Sci. and Technol.*, vol. 45, no. 5, pp. 444-450(2001).
- 5) N. Tsumura, N. Ojima, K. Sato, M. Shiraiishi, H. Shimizu, H. Nabeshima, S. Akazaki, K. Horii and Y Miyake, *ACM Trans. Graph.*, vol. 22, pp. 770-779, (2003).
- 6) M. Nishibori, N. Tsumura, Y. Miyake, *J. Imaging Sci. and Technol.*, vol. 48, no. 2, pp. 125-129(2004).
- 7) N. Tsumura, in 23rd Annual Meeting of the IEEE Photonics Society, Colorado, USA, (November 7-11 2010).
- 8) S. Yamamoto, N. Tsumura, T. Nakaguchi, T. Namiki, Y. Kasahara, K. Terasawa and Y. Miyake, *Int. J. Comput. Assist. Radiol. Surg.*, vol. 6, pp. 143-152, (2011).
- 9) M. Hirose, R. Akaho, C. Maita, M. Kuroshima and N. Tsumura, in 11th Finland-Japan Joint Symposium on Optics in Engineering (OIE 2015). Joensuu, Finland, (September 1-3 2015).
- 10) K. Kikuchi, Y. Masuda, T.Hirao, *Skin Research and Technol.*, vol. 19, pp. 499-507, (2013).
- 11) M. Kobayashi, Y. Ito, N. Sakauchi, I. Oda, I. Konishi and Y. Tsunazawa, 'Analysis of nonlinear relation for skin hemoglobin imaging,' *pt. Exp.*, vol. 9, pp. 802-812, 2001.
- 12) M. Hirose, M. Kuroshima and N. Tsumura, 'Nonlinear Estimation of Chromophore Concentrations, Shading and Surface Reflectance from Five Band Images,' in 23rd Color and Imaging Conference (CIC 23). Darmstadt, Germany, October 19-23 2015.
- 13) Steven L. Jacques, 'Skin Optics', <http://omlc.ogi.edu/news/jan98/skinoptics.html> (Oregon Medical Laser Center News. Jan 1998.), (1998)
- 14) G. Poirier, 'Human skin modelling and rendering,' aster's thesis (University of Waterloo, 2004), (2004).

Caption of Fig.s

Fig.1 Two-layered skin model is composed of the epidermis and dermis.

Fig.2 Skin absorbance $Z(\lambda)$. (a) shows skin absorbance at 400nm. (b) 500nm. (c) 600nm. (d) 700nm.

Fig.3 Flow of estimation method.

Fig.4 Experimental set-up.

Fig.5 RGB Image of skin.

Fig.6 Concentration distribution of chromophore at spot on the skin by using proposed method. (a) shows RGB image. (b) shows melanin map. (c) shows shading map. (d) shows oxygen saturation map. (e) shows blood volume map.

Fig.7 Concentration distribution of chromophore at spot on the skin by using conventional multiple regression analysis. (a) shows RGB image. (b) shows melanin map. (c) shows shading map. (d) shows oxygen saturation map. (e) shows blood volume map.

Fig.8 Concentration distribution of chromophore at dark circles under the eyes by using proposed method. (a) shows RGB image. (b) shows melanin map. (c) shows shading map. (d) shows oxygen saturation map. (e) shows blood volume map.

Fig.9 Concentration distribution of chromophore at dark circles under the eyes by using conventional multiple regression analysis. (a) shows RGB image. (b) shows melanin map. (c) shows shading map. (d) shows oxygen saturation map. (e) shows blood volume map.

Fig.10 Modulation of melanin concentration and RGB image.

Fig.11 Modulated image related to melanin and blood volume.

Fig.12 Modulated image related to melanin and oxygen saturation.

Fig.13 Modulated image related to melanin and shading.

Fig.14 Subjective evaluation experiment

Fig.15 Result of subjective evaluation experiment.

Fig.16 Removal of dark circle by decreasing melanin. (a) shows RGB image before modulation. (b) shows RGB image after decreasing melanin.

Tables

Table. 1 The evaluation is performed by classification with five grades.

Evaluation value	
5	Improvement
4	Little improvement
3	No-change
2	Little aggravation
1	Aggravation

Figures

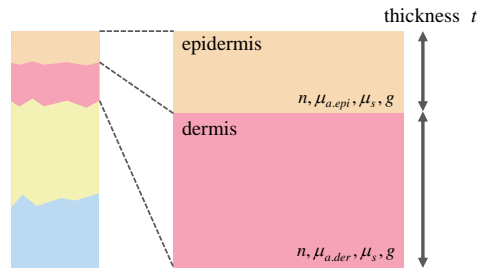


Fig. 1

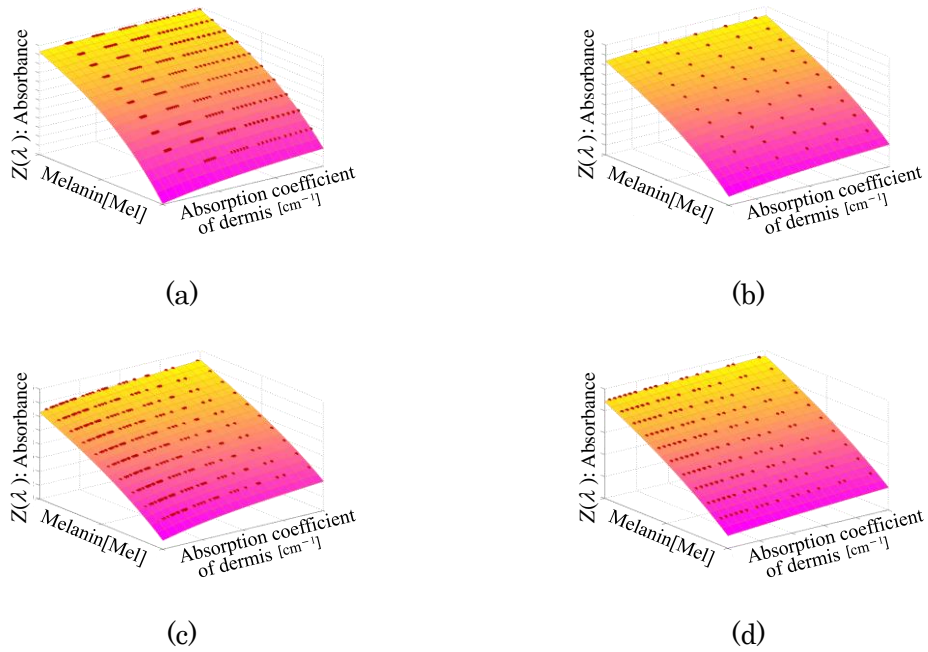


Fig. 2

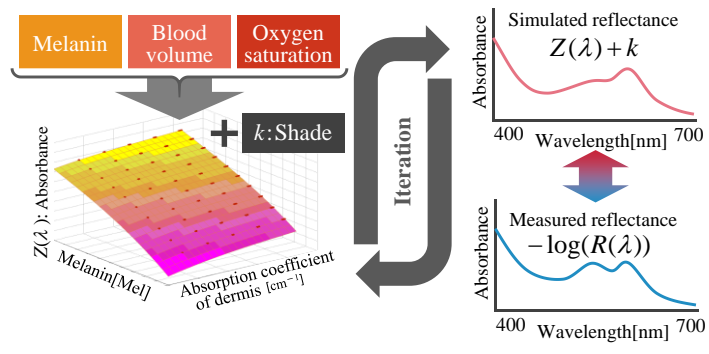


Fig. 3

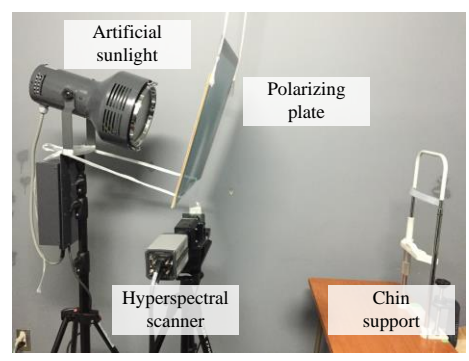


Fig. 4

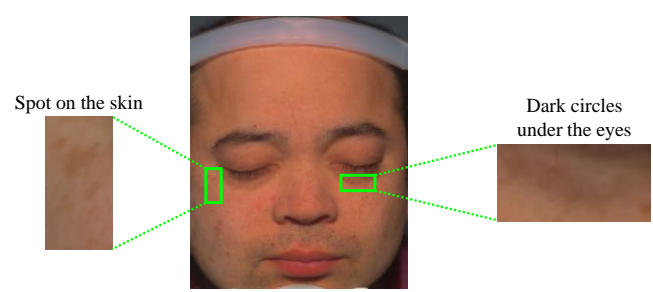


Fig. 5

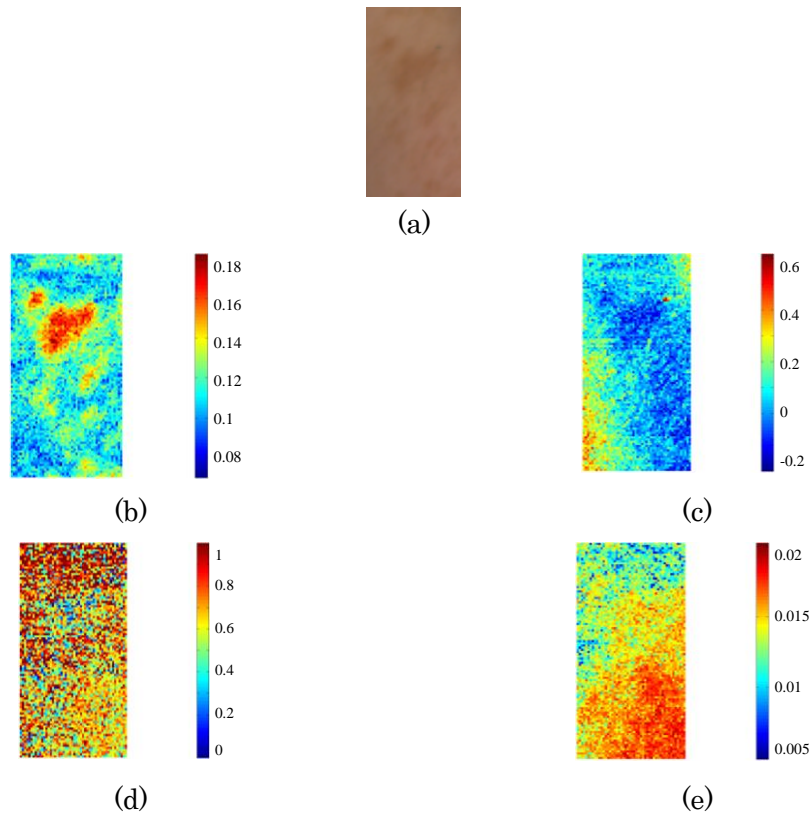


Fig. 6

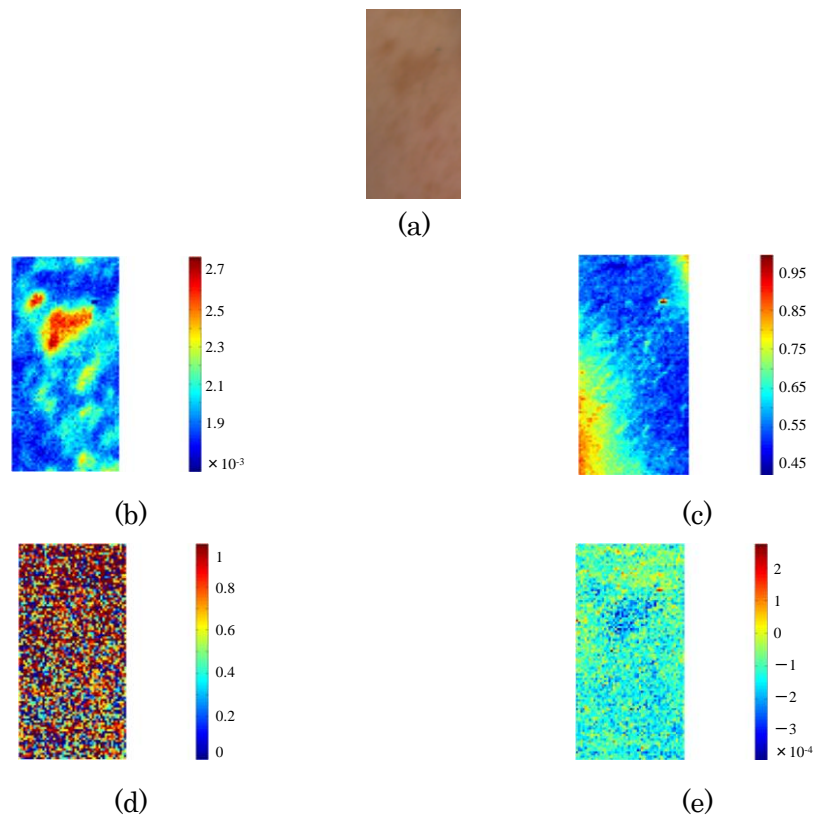


Fig. 7

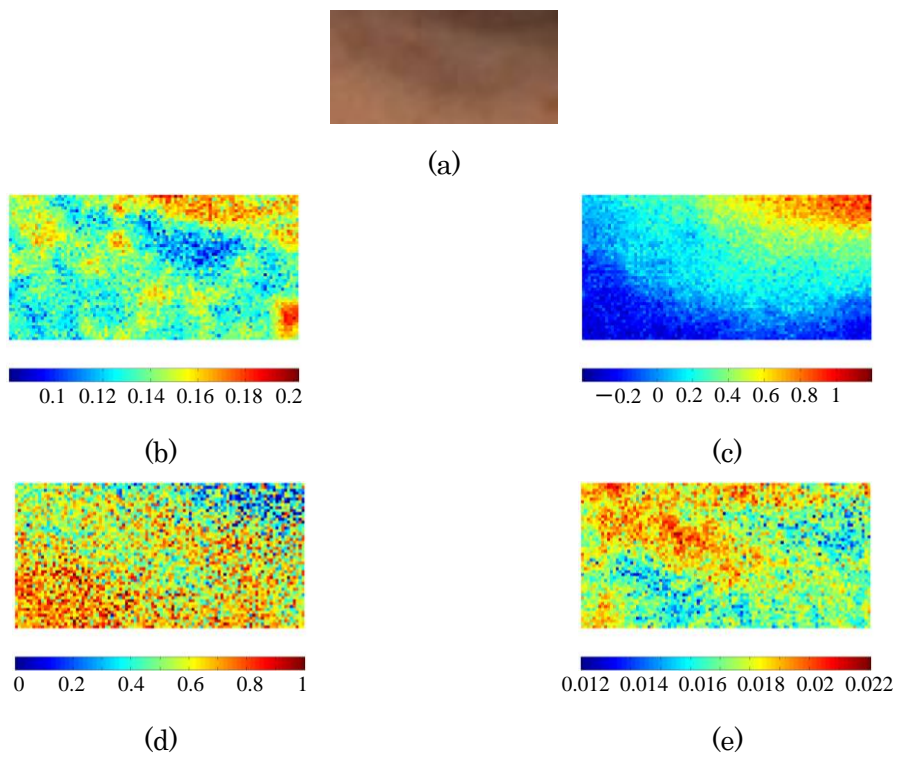


Fig. 8

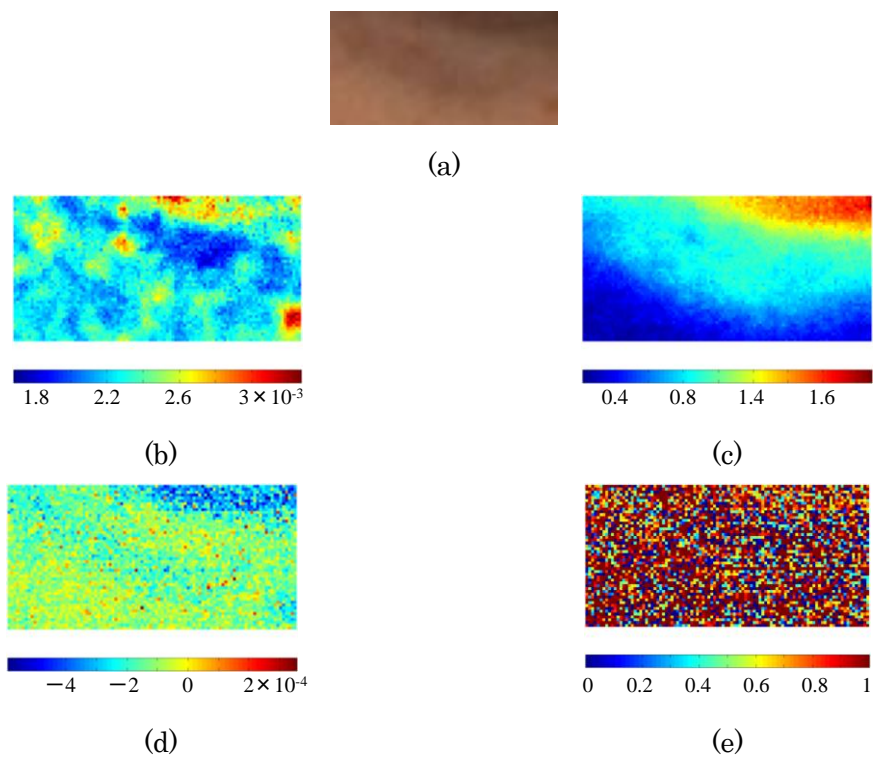


Fig. 9

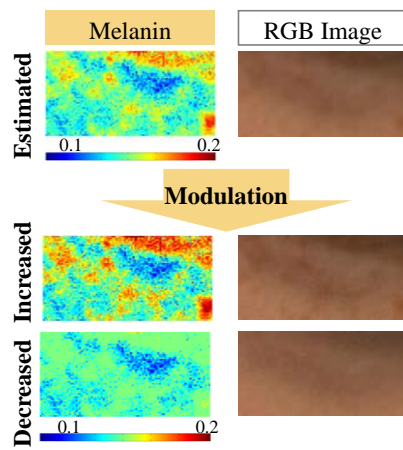


Fig. 10

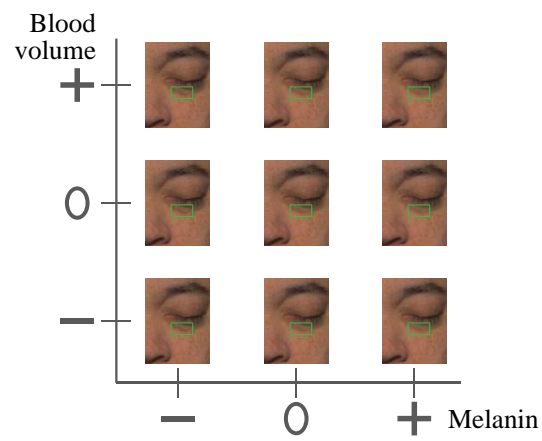


Fig. 11

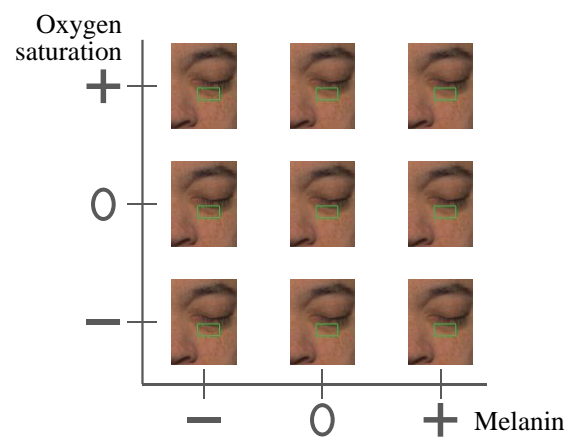


Fig. 12

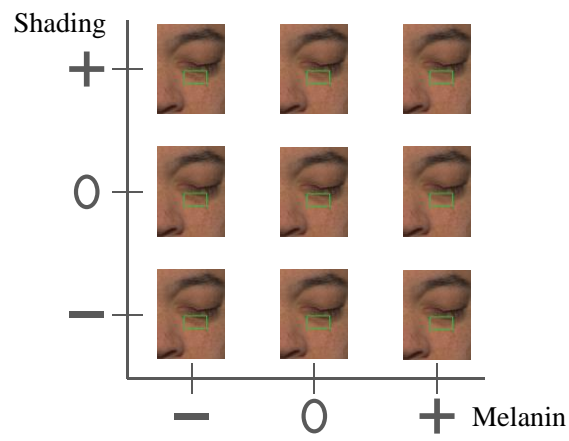
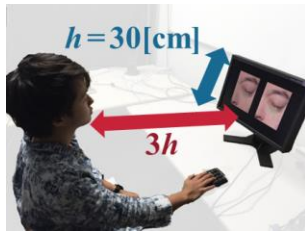
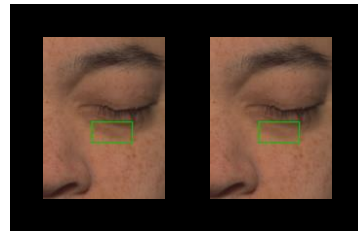


Fig. 13



(a)



(b)

Fig. 14

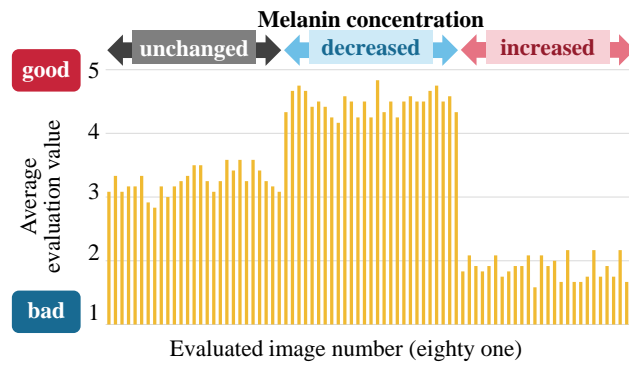
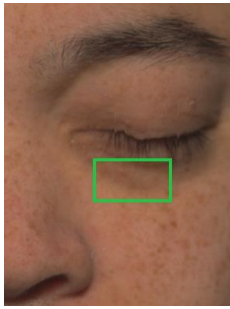
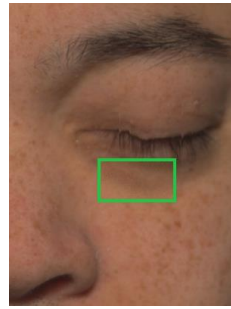


Fig. 15



(a)



(b)

Fig. 16